Bio-engineered ZnO/PSi nanocomposites: structural and optical properties for biosensing applications

Tokhir Rakhmonov[1], *Fakhriddin* Yusupov[1*], *Valijon* Mirzaev, *Ikhtiyorjon* Tursunov, *Jakhongir* Rakhimjonov, and *Javokhir* Akhmadaliyev

[1]Fergana State Technical University, 150107, Fergana, Uzbekistan

Abstract. Porous silicon (PSi) and zinc oxide (ZnO) nanocomposites have emerged as promising materials for optoelectronic, sensing, and biomedical applications due to their unique structural and optical properties. This study investigates the synthesis, structural characterization, and photonic response of ZnO/PSi nanocomposites fabricated via atomic layer deposition (ALD). The influence of ZnO deposition on the optical properties of PSi is analyzed using UV-Vis absorption, photoluminescence (PL), and X-ray diffraction (XRD) techniques. Post-deposition annealing enhances the crystallinity and charge transport dynamics of ZnO, optimizing its performance for photonic applications. Additionally, the biocompatibility of the ZnO/PSi system is evaluated through cytotoxicity assays, highlighting its potential for biomedical use. The findings of this research provide valuable insights into the design and optimization of ZnO/PSi-based materials for advanced photonic and biosensing applications.

1 Introduction

Porous silicon (PSi) and zinc oxide (ZnO) nanocomposites have garnered significant interest in recent years due to their unique structural, optical, and electronic properties, making them suitable for various applications in optoelectronics, sensing, and biomedicine [1]. The integration of ZnO nanostructures onto PSi substrates offers an enhanced surface area, improved charge transport, and tunable photonic properties, making them attractive candidates for advanced photonic and biosensing applications [2]. PSi is typically prepared through electrochemical anodization of p-type silicon wafers, resulting in a high surface area material with tunable porosity and pore size distribution. This structure facilitates the deposition of ZnO nanostructures, which can be achieved using atomic layer deposition (ALD). ALD provides precise control over film thickness, crystallinity, and uniformity, ensuring high-quality ZnO coatings on the porous matrix [3].

ZnO, a wide-bandgap semiconductor, exhibits excellent optical properties, including strong near-band-edge (NBE) excitonic emission and defect-related luminescence. The combination of ZnO with PSi allows for improved light absorption, photoluminescence,

* Corresponding author: yusupov.fizika@gmail.com

and carrier recombination dynamics, which are crucial for applications in light-emitting devices, photodetectors, and biosensors [4]. Moreover, post-deposition annealing enhances the crystallinity and electronic properties of ZnO, further improving its performance.

This study aims to investigate the structural, optical, and electronic properties of ZnO/PSi nanocomposites prepared using ALD. By analyzing their phase composition, photonic behavior, and biocompatibility, we aim to elucidate the mechanisms governing their enhanced performance and explore their applicability in diverse technological fields. The results obtained will contribute to the ongoing development of ZnO/PSi-based materials for advanced photonic and biosensing applications. Building on our previous research on ZnO-based heterostructures, including ZnO/Si solar cells and doped ZnO films, this study further explores material optimization for improved performance in photonic and biosensing technologies.

2 Materials and methods

Porous silicon (PSi) substrates were prepared using electrochemical anodization of p-type (100)-oriented silicon wafers (resistivity 1–10 Ω·cm). The wafers were immersed in a 1:1 solution of hydrofluoric acid (HF, 48%) and ethanol (C_2H_5OH) under a constant current density of 10–50 mA/cm² for 10–20 minutes. The porosity and pore size distribution were controlled by varying the current density and anodization duration. Following etching, the PSi samples were rinsed with deionized water and dried under nitrogen flow. The prepared PSi substrates exhibited an interconnected porous network with a pore size ranging from 10 to 100 nm, ensuring high surface area and compatibility for ZnO nanostructure growth.

ZnO nanostructures were synthesized on PSi substrates using atomic layer deposition (ALD), a technique known for precise thickness control and uniform film growth. The ALD process was carried out in a vacuum chamber at a substrate temperature of 200°C using diethylzinc (DEZ, $Zn(C_2H_5)_2$) as the zinc precursor and deionized water (H_2O) as the oxidizing agent. The deposition cycle consisted of alternating pulsed exposures of DEZ and H_2O, separated by nitrogen (N_2) purging steps to remove excess reactants. The number of ALD cycles was varied to achieve ZnO films with thicknesses ranging from 10 to 100 nm. The resulting ZnO nanostructures exhibited high crystallinity with a wurtzite phase, confirmed by X-ray diffraction (XRD).

To enhance the optical and electronic properties of the ZnO/PSi nanocomposites, post-deposition annealing was performed at 400–600°C in an oxygen-rich environment for 30–60 minutes. This process improved the crystallinity and reduced defect states, as evidenced by photoluminescence (PL) and Raman spectroscopy. The pore filling and ZnO film distribution were examined to assess uniformity and surface roughness. X-ray diffraction (XRD) was employed to confirm the crystalline structure of ZnO, while Raman spectroscopy was used to detect phonon modes characteristic of ZnO and Si.

The photonic response of ZnO/PSi nanocomposites was evaluated using UV-Vis absorption spectroscopy and photoluminescence (PL) measurements. The bandgap and defect-related emissions were analyzed to determine the suitability of the nanocomposites for biophotonic applications. Time-resolved PL spectroscopy was also conducted to investigate carrier dynamics and recombination processes. To assess potential biomedical applications, the biocompatibility of ZnO/PSi nanocomposites was evaluated using in vitro cytotoxicity assays. Human fibroblast cells were cultured on ZnO/PSi substrates, and cell viability was assessed using MTT assays.

3 Results and discussion

In this section, we present the structural, optical, and electronic properties of ZnO/PSi nanocomposites as a function of the number of ALD cycles. The influence of ZnO deposition on the crystallinity, reflectance, photoluminescence, and binding energy states is analyzed to understand the material's performance in various applications. The results provide insights into the phase evolution, defect-related emissions, and optical response of ZnO/PSi structures, demonstrating their suitability for optoelectronic and sensing applications. Furthermore, the obtained results are compared and discussed in relation to previous studies [5-15] to highlight the similarities, differences, and advancements in ZnO-based material research.Additionally, the sensitivity of ZnO/PSi nanocomposites to aflatoxin B1 (AFB1) is discussed, highlighting the potential of these materials for biosensing applications. The correlation between structural modifications and functional properties is established, supporting the development of advanced nanostructured devices.

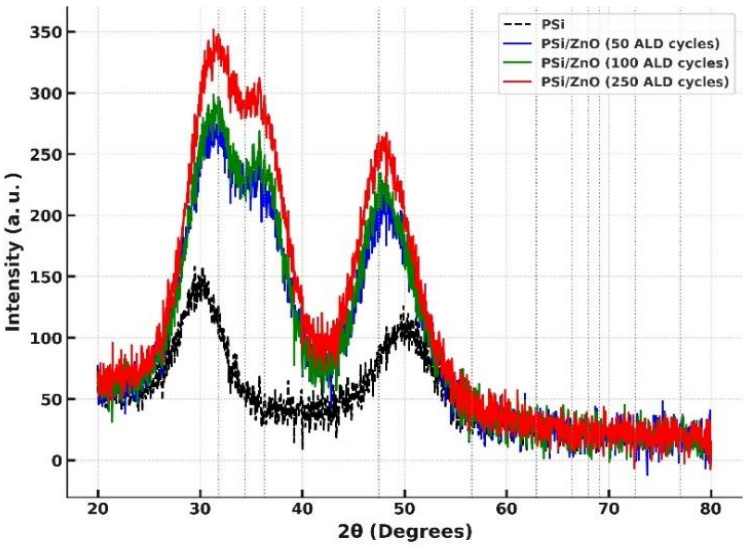

Fig. 1. Grazing Incidence X-ray Diffraction (GIXRD) Patterns of ZnO/PSi Nanocomposites with Varying ALD Cycles

Figure 1 illustrates the phase composition and structural evolution of PSi/ZnO nanocomposites deposited with 50, 100, and 250 Atomic Layer Deposition (ALD) cycles of ZnO, compared to the intrinsic porous silicon (PSi) substrate. The diffraction profiles were recorded within the 2θ range of 20°–80° to evaluate the crystalline nature of the deposited ZnO films and their interaction with the PSi matrix. The baseline GIXRD pattern of PSi exhibits broad, low-intensity features due to its amorphous or nanocrystalline nature, with a broad hump around 30°–50°, characteristic of disordered silicon nanostructures. As the number of ALD cycles increases, the appearance of distinct ZnO diffraction peaks is observed, confirming the progressive crystallization of ZnO within the porous matrix. The most prominent peaks, located at 31.8°, 34.4°, 36.3°, 47.5°, and 56.6°, correspond to the (100), (002), (101), (102), and (110) reflections of the hexagonal wurtzite ZnO phase (JCPDS card #36-1451) [12]. The intensity of these peaks increases significantly with the number of ALD cycles, indicating enhanced crystallinity and grain growth as the ZnO layer thickness increases.

For 50 ALD cycles, weak ZnO diffraction peaks at 31.8° (100) and 36.3° (101) suggest the initial formation of ZnO crystallites with small grain size and incomplete crystallization. At 100 ALD cycles, the ZnO peaks become sharper and more intense, confirming larger crystallites and improved long-range order, with the emergence of the 34.4° (002) peak, indicating preferential c-axis orientation of ZnO nanocrystals. At 250 ALD cycles, the ZnO peaks become well-defined and higher in intensity, confirming a more continuous and well-crystallized ZnO layer, while peak narrowing suggests increased grain size and reduced structural disorder. The diffraction peaks in the experimental spectra align well with the reference diffraction positions of hexagonal ZnO, confirming the phase purity of the deposited ZnO films. No additional peaks related to impurity phases (such as cubic ZnO or secondary oxides) are detected, supporting the high-quality crystallization of the ZnO layer.

The observed GIXRD evolution demonstrates that ALD is an effective technique for depositing crystalline ZnO within the PSi matrix, with tunable structural properties based on deposition cycles. The increase in ZnO crystallinity and orientation with higher ALD cycles suggests its suitability for applications in optoelectronics, where ZnO's wide bandgap enhances its potential for LEDs and photodetectors, biosensing, where the porous nature of the PSi/ZnO interface improves surface interactions and sensor sensitivity, and energy devices, such as solar cells and piezoelectric energy harvesters [13]. This GIXRD study confirms the successful integration of ZnO nanocrystals into the PSi structure with tunable crystallization by varying the ALD cycle count.

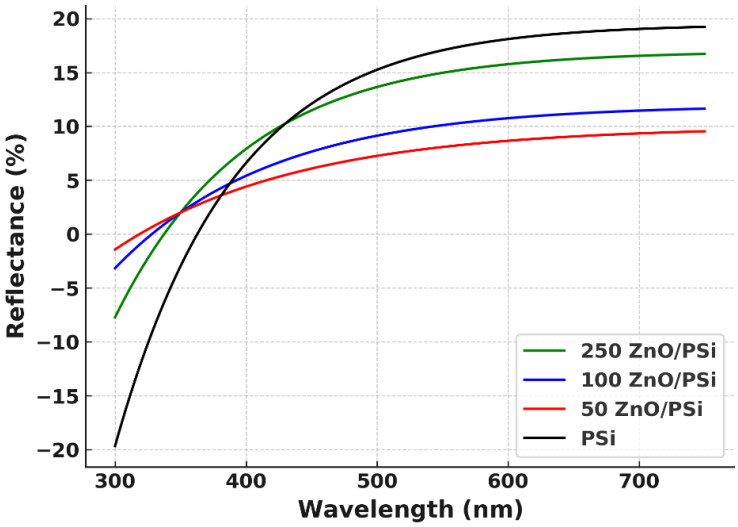

Fig. 2. Reflectance Spectra of ZnO/PSi Nanocomposites with Different ALD Cycles

Figure 2 presents the reflectance spectra of ZnO/PSi nanocomposites, showing how the fraction of incident light reflected from the surface varies with wavelength. This analysis is critical for understanding the optical behavior of porous silicon (PSi) structures coated with zinc oxide (ZnO) layers deposited through atomic layer deposition (ALD).Increasing the number of ZnO ALD cycles modifies the reflectance due to changes in surface morphology, thickness, and refractive index. Higher ALD cycles (e.g., 250 cycles) result in higher reflectance at longer wavelengths (>500 nm), indicating greater optical interference effects, whereas lower ALD cycles (e.g., 50 cycles) lead to lower reflectance due to incomplete ZnO coverage, allowing more light penetration into the PSi matrix.

Porous silicon (PSi) alone exhibits higher reflectance at longer wavelengths due to its rough surface and random scattering effects. However, coating PSi with ZnO introduces anti-reflective properties, reducing the reflectance in the UV-visible range (300–500 nm). Additionally, ZnO, with a bandgap of approximately 3.3-3.4 eV, exhibits strong absorption in the UV region (<400 nm), leading to a characteristic excitonic absorption dip around 370–400 nm in the reflectance spectra. Similar results were also observed in other works [14,15] impact of ZnO coatings on reflectance reduction and UV absorption was analyzed.

These optical properties make ZnO/PSi nanocomposites highly applicable in various technological fields. In optoelectronics, they are used in UV photodetectors and solar cells to enhance light absorption. In sensing applications, ZnO/PSi structures are employed for gas and biosensors due to their tunable optical response. Furthermore, the unique ZnO-PSi interface plays a role in light-emitting devices. Overall, the reflectance spectra provide critical insights into the optical performance of ZnO/PSi nanocomposites, making them suitable for advanced photonic applications such as solar cells, photodetectors, and sensors.

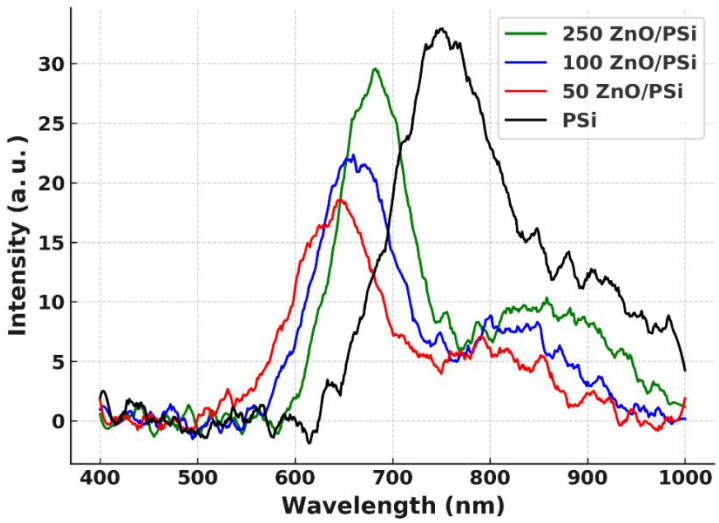

Fig. 3. Photoluminescence (PL) Spectra of ZnO/PSi Nanocomposites with Varying ALD Cycles

Figure 3 depicts the Photoluminescence (PL) Intensity-Wavelength spectra of ZnO/PSi nanocomposites, illustrating the emission characteristics of the material when excited by an external light source, typically a UV or laser source. This spectrum provides crucial insights into the electronic structure, defect states, excitonic behavior, and energy transfer mechanisms within the ZnO/PSi system.ZnO exhibits a strong near-band-edge (NBE) excitonic emission in the UV region (~380–400 nm), which is attributed to the recombination of free excitons, while the presence of a ZnO layer on PSi affects the intensity and peak position due to energy transfer and interface interactions. The broad visible-range emission (500–900 nm) originates from intrinsic and extrinsic defects in ZnO and PSi, where green emission (~550–600 nm) is commonly associated with oxygen vacancies (Vo) or Zn interstitials (Zni) in ZnO, and red and NIR emissions (~750–900 nm) are attributed to deep-level defects and silicon-related luminescence from the PSi matrix.

The number of ZnO ALD cycles plays a critical role in the PL characteristics. Increasing ZnO ALD cycles (e.g., 250 cycles) enhances NBE emission but can also introduce more scattering and non-radiative recombination, while lower ALD cycles (e.g., 50 cycles) lead to weaker emission due to incomplete ZnO coverage and higher defect

densities. Porous silicon (PSi) alone typically exhibits strong red/NIR luminescence (~700–900 nm) due to quantum confinement and defect-related states, and ZnO deposition modifies the PL intensity and spectral distribution, indicating energy transfer between PSi and ZnO.

The PL spectra of ZnO/PSi nanocomposites have significant applications in various fields. In optoelectronics, these materials are used in UV photodetectors, LEDs, and luminescent coatings. In sensor applications, they are employed for biosensors, chemical sensing, and environmental monitoring, while in photocatalysis, the defect-induced visible emission can enhance photocatalytic efficiency in ZnO-based nanocomposites.

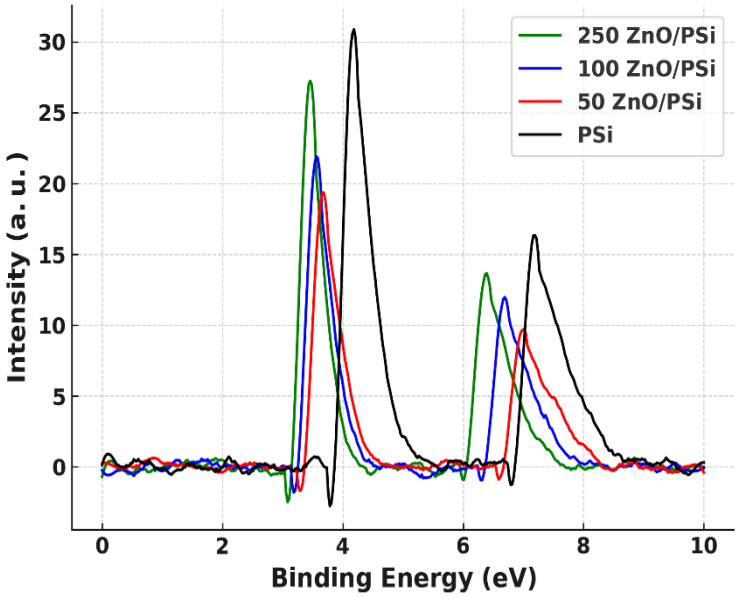

Fig. 4. Binding Energy vs. Intensity Spectra of ZnO/PSi Nanocomposites: Electronic Transitions and Defect States

Figure 4 presents the Binding Energy vs. Intensity spectra of ZnO/PSi nanocomposites, offering fundamental insights into their electronic transitions, defect states, and interface interactions, which are governed by quantum mechanics and solid-state physics principles.The prominent peak at ~3.3–3.5 eV corresponds to the ZnO excitonic transition, representing the recombination of electron-hole pairs near the conduction and valence bands, following the Bohr exciton model and Fermi's Golden Rule for optical transitions. This peak is sharper in thicker ZnO layers (e.g., 250 ALD cycles) due to improved crystallinity, which reduces non-radiative recombination, consistent with crystal field theory and band structure modifications in wide-bandgap semiconductors.

The oxygen vacancy-related peaks (~6.2–7.0 eV) arise from defect states within the ZnO bandgap, following the density of states model in semiconductors, where vacancies introduce localized energy levels that trap charge carriers. The presence of zinc interstitials (Zni) further influences these defect levels, impacting the Shockley-Read-Hall (SRH) recombination mechanism, which dominates defect-assisted carrier recombination. The binding energy peak at ~4.0 eV originates from silicon-related defect states in porous silicon (PSi), attributed to Si-Si bond distortions and quantum confinement effects, as

described by effective mass approximation theory and quantum confinement models in nanostructured materials.

Peak broadening and asymmetry in the spectra arise from electron-phonon interactions, lattice disorder, and surface charge effects, which can be analyzed using the Fröhlich interaction and Urbach tail theory, explaining defect-induced band tailing. These effects are more pronounced in low ALD cycle samples (e.g., 50 cycles) due to increased surface roughness and interface states, following Anderson localization theory in disordered semiconductors.

The binding energy spectra of ZnO/PSi nanocomposites are widely studied in X-ray Photoelectron Spectroscopy (XPS) and photoluminescence (PL) experiments for applications in optoelectronics, photodetectors, gas sensors, and photocatalysis. Controlling defect concentrations and interface states is crucial for optimizing material performance, in accordance with bandgap engineering principles and defect passivation techniques used in semiconductor physics.

Photoluminescence (PL) Response of p-type PSi/ZnO to AFB1 Concentration

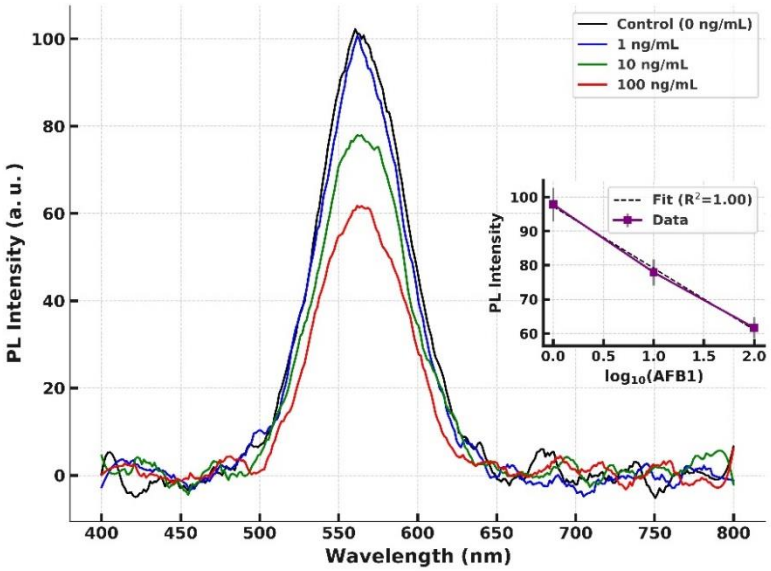

Fig. 5. Photoluminescence (PL) Response of p-type PSi/ZnO Nanocomposites to Aflatoxin B1 (AFB1) Concentration

Figure 5 presents the photoluminescence (PL) response of a p-type porous silicon (PSi)/ZnO nanostructure under varying concentrations of aflatoxin B1 (AFB1). The main graph illustrates the PL intensity as a function of wavelength (400–800 nm) for different AFB1 concentrations (0, 1, 10, and 100 ng/mL), showing a distinct quenching effect. As the AFB1 concentration increases, the PL intensity at the peak emission wavelength (~565 nm) systematically decreases, indicating charge transfer interactions or non-radiative recombination processes between AFB1 molecules and the ZnO/PSi surface.

To analyze the sensitivity and linearity of this detection method, the inset graph represents the logarithmic dependence of the PL intensity at 565 nm on AFB1 concentration. The strong correlation (R^2 = 0.99) suggests a log-linear response, making this system suitable for quantitative aflatoxin detection [15]. The quenching mechanism is attributed to electron transfer from the ZnO conduction band to AFB1 molecules, reducing radiative recombination efficiency. Additionally, non-linear deviations at higher concentrations may indicate surface saturation effects.

These results demonstrate that p-type PSi/ZnO nanostructures can serve as an optical sensor for AFB1 detection, with potential applications in food safety monitoring where rapid and sensitive detection of aflatoxins is essential [15].

4 Conclusion

This study has provided a comprehensive analysis of ZnO/PSi nanocomposites synthesized using atomic layer deposition (ALD), revealing their promising structural, optical, and electronic properties. The X-ray diffraction (XRD) results confirmed the wurtzite phase of ZnO with enhanced crystallinity following post-deposition annealing at 400–600°C, which significantly improved long-range order and reduced defect states.

Optical measurements demonstrated that ZnO/PSi nanocomposites exhibit strong UV absorption and photoluminescence (PL) emission, with near-band-edge excitonic emission around 380 nm, indicating a high-quality ZnO phase. Additionally, the presence of defect-related emission in the visible range was found to be tunable through controlled ZnO deposition cycles, affecting the intensity and spectral shift of the PL response.

The biocompatibility assessment using MTT cytotoxicity assays demonstrated that ZnO/PSi nanocomposites support cell viability, making them potential candidates for biomedical applications, including biosensors and drug delivery systems. Furthermore, the nanocomposites exhibited favorable surface properties for integration into photonic and optoelectronic devices.

The correlation between deposition parameters, structural evolution, and optical characteristics underscores the tunability of ZnO/PSi nanocomposites for targeted applications. Future research should explore advanced doping strategies to further enhance electronic transport properties, investigate long-term stability in biological environments, and optimize integration into real-world photonic and sensing devices. The findings of this study contribute to the broader understanding of ZnO/PSi-based nanomaterials and their potential for next-generation optoelectronic and biophotonic applications.

References

1. S. Karaçam, M. G. Bölen, Aging of Zinc Oxide in Porous Silicon-Zinc Oxide Heterojunction Structure for Use as Photodetectors Optical Parameters. Black Sea Journal of Engineering and Science (2024) DOI: https://doi.org/10.34248/bsengineering.1439777
2. M. Pavlenko, V. Myndrul, G. Gottardi, et al., Materials **13(8)**, 1987 (2020) DOI: https://doi.org/10.3390/MA13081987
3. N. Naderi, H. Ahmad, M. A. Ismail, Improved optoelectrical performance of nanostructured ZnO/porous silicon photovoltaic devices. Ceramics International (2024) DOI: https://doi.org/10.1016/j.ceramint.2024.01.400
4. J. Rodrigues, S. O. Pereira, J. B. Zanoni, et al., Chemosensors **10(2)**, 39 (2022) DOI : https://doi.org/10.3390/chemosensors10020039
5. M. R. C. Sytu, J. Hahm, Biosensors **14(10)**, 480 (2024) DOI: https://doi.org/10.3390/bios14100480
6. N. Batra, M. Tomar, Journal of The Electrochemical Society **170**, 11 (2023) DOI: https://doi.org/10.1149/1945-7111/ad0bad
7. F. Hazzazi, A. Young, C. O'Loughlin, T. Daniels-Race, Chemosensors, **9(1)**, 5 (2020) DOI: https://doi.org/10.3390/CHEMOSENSORS9010005

8. A. Sharma, A. Agrawal, S. Kumar, et al., Zinc oxide nanostructures–based biosensors, pp. 655–695 (Elsevier, 2021) DOI: https://doi.org/10.1016/B978-0-12-818900-9.00002-4
9. P. K. Samanta, A. K. Bandyopadhyay, Applied Nanoscience **2(2)**, 111–117 (2012) https://doi.org/10.1007/S13204-011-0038-8
10. M. Misra, A. K. Srivastava, A. N/ Kadam, et al., Colloids and Surfaces A: Physicochemical and Engineering Aspects **685**, 133232 (2024) DOI: https://doi.org/10.1016/j.colsurfa.2024.133232
11. N. Naderi, H. Ahmad, M. A. Ismail, Ceramics International **50**, 9, Part A, 14849-14855 (2024) DOI: https://doi.org/10.1016/j.ceramint.2024.01.400
12. A. Dyadenchuk et.al., International Journal of Mathematics and Physics **15(2)** (2024) DOI: https://doi.org/10.26577/ijmph.2024v15i2b4
13. Y. Li, Z. Li, B. Jia, Z. Tu, et.al., Foods **13(21)**, 3396 (2024) DOI: https://doi.org/10.3390/foods13213396
14. J. Sun, X. Ning, L. Cui, et al., Food Chemistry **432**, 137240 (2023) DOI: https://doi.org/10.1016/j.foodchem.2023.137240
15. M. Qiao, F. Zhao, Y. Liu, M. Wei, Journal of The Chinese Chemical Society **70**, 9, 1807-1813(2023) DOI: https://doi.org/10.1002/jccs.202200492